X-ray Photoelectron Spectroscopy Analyses of the Electronic Structure of Polycrystalline $Ti_{1-x}Al_xN$ Thin Films with $0 \leq x \leq 0.96$

Grzegorz Greczynski[a] and Jens Jensen
Linköping University, Department of Physics (IFM), Linköping, 581 83, Sweden

J. E. Greene and Ivan Petrov
University of Illinois, Materials Science Department and Frederick Seitz Materials Research Laboratory, Urbana, IL 61801

Lars Hultman
Linköping University, Department of Physics (IFM), Linköping, 581 83, Sweden

(Received 27 May 2014; accepted 19 August 2014; published 24 October 2014)

Metastable $Ti_{1-x}Al_xN$ ($0 \leq x \leq 0.96$) alloy thin films are grown by reactive magnetron sputter deposition using a combination of high-power pulsed magnetron (HIPIMS) and DC magnetron sputtering (DCMS). Layers are deposited from elemental Ti and Al targets onto Si(001) substrates at 500 °C. All $Ti_{1-x}Al_xN$ film surfaces are analyzed by x-ray photoelectron spectroscopy (XPS) employing monochromatic Al K_α radiation (h_ν = 1486.6 eV). Prior to spectra acquisition, TiAlN surfaces are sputter-cleaned in-situ with 4 keV Ar^+ ions incident at an angle of 70° with respect to the surface normal. XPS results reveal satellite structures on the high binding energy side of the Ti 2p, Ti 3s, and Ti 3p core-level signals. The intensities of the primary Ti features (Ti 2p, Ti 3s, and Ti 3p) decrease with increasing AlN concentration such that the satellite peaks dominate spectra from films with $x \geq 0.67$. The density-of-states at the Fermi level also decrease with increasing x indicating that the satellite peaks are due to screening of core holes created by the photoionization event. Film compositions, obtained using XPS sensitivity factors, agree to within ±3% with values determined by time-of-flight elastic recoil detection analyses. © *2014 American Vacuum Society*. [http://dx.doi.org/10.1116/11.20140506]

Keywords: *HIPIMS; TiAlN; magnetron sputtering; XPS; hard coatings; transition metal nitride*

Accession #s: 01289, 01290, 01291, 01292, 01293, 01294, 01295, 01296, 01297, 01298, 01299, 01300, 01301

Technique: XPS

Host Material: #01289: TiN; #01290: $Ti_{0.84}Al_{0.16}N$; #01291: $Ti_{0.74}Al_{0.26}N$; #01292: $Ti_{0.65}Al_{0.35}N$; #01293: $Ti_{0.59}Al_{0.41}N$; #01294: $Ti_{0.46}Al_{0.54}N$; #01295: $Ti_{0.41}Al_{0.59}N$; #01296: $Ti_{0.33}Al_{0.67}N$; #01297: $Ti_{0.27}Al_{0.73}N$; #01298: $Ti_{0.24}Al_{0.76}N$; #01299: $Ti_{0.20}Al_{0.80}N$; #01300: $Ti_{0.08}Al_{0.92}N$; #01301: $Ti_{0.04}Al_{0.96}N$

Instrument: Kratos Analytical Axis Ultra DLD

Major Elements in Spectra: Ti, Al, N

Minor Elements in Spectra: O

Published Spectra: 104

Spectra in Electronic Record: 104

Spectral Category: reference

INTRODUCTION

Thin films of metastable NaCl-structure $Ti_{1-x}Al_xN$ exhibiting high hardness and good high-temperature oxidation resistance are of increasing scientific and technological interest due to applications ranging from wear-resistant coatings on high-speed cutting tools (Refs. 1 and 2) to use as bio-implant coatings (Ref. 3). Enhanced high-temperature performance is obtained for alloy films with high AlN contents. Film growth parameters have been shown to dramatically affect kinetic solid solubilities of wurtzite-structure AlN in cubic TiN (Ref. 4). At thermodynamic equilibrium, the solubility of AlN in TiN is only 2 mol% at 1000 °C (Ref. 5) and increases to 5 mol% at 2425 °C (Ref. 6). Calculated $Ti_{1-x}Al_xN$ mixing enthalpies are positive over the entire composition range and reach a maximum at $x = 0.68$ (Ref. 7). Nevertheless, metastable NaCl-structure pseudobinary alloys can be obtained by physical vapor deposition (PVD) due to kinetically-limited low-temperature growth and low-energy ion-irradiation-induced dynamic mixing in the near-surface region. Reported kinetic AlN solubility limits in cubic $Ti_{1-x}Al_xN$ alloys are typically $x_{max} \sim 0.50$ for dc magnetron sputter (DCMS) deposition at film growth temperatures T_s = 500 °C (Refs. 8 and 9), while x_{max} values up to 0.66 have been reported using cathodic arc evaporation (Refs. 10 and 11). However, the resulting films have very high compressive stresses, up to −5 GPa (Ref. 12) for DCMS and −9.1 GPa (Ref. 13) for arc-deposited films.

Recently, we have shown that single-phase NaCl-structure $Ti_{1-x}Al_xN$ alloys with $x \leq 0.64$, combining high hardness and low residual stress, can be grown by a hybrid technique consisting of reactive high-power pulsed magnetron sputtering (HIPIMS) of Al and DC magnetron sputtering (DCMS) of Ti targets (Al-HIPIMS/Ti-DCMS) (Refs. 14–16). In distinct contrast, Ti-HIPIMS/Al-DCMS $Ti_{1-x}Al_xN$ layers with $x > 0.41$ are two-phase mixtures, NaCl-structure $Ti_{1-x}Al_xN$ plus wurtzite AlN, which exhibit low hardness with high compressive stress due to an intense energetic Ti^{2+} metal-ion flux incident at the growing film surface.

Here, we employ x-ray photoelectron spectroscopy (XPS) to investigate the electronic structure of $Ti_{1-x}Al_xN$ alloy thin films with $0 \leq x \leq 0.96$ grown by reactive hybrid Ti-HIPIMS/Al-DCMS co-sputtering. Film compositions are determined by time-of-flight elastic recoil detection analyses (ToF-E ERDA) (Ref. 17) with a 40 MeV $^{127}I^{9+}$ probe beam incident at 67.5° with respect to the sample surface normal; recoils are detected at 45°.

X-ray diffraction (XRD) and transmission electron microscopy (TEM) analyses reveal that $Ti_{1-x}Al_xN$ films with $x \leq 0.41$ are 002-oriented polycrystalline, NaCl-structure, single-phase alloys. Films with composition $0.53 \leq x \leq 0.67$ have a two-phase, cubic plus wurtzite, structure with random orientation; films with $x \geq 0.73$ have the wurtzite structure. XPS analyses are carried out with monochromatic Al K_α radiation (h_ν = 1486.6 eV) following sample sputter-cleaning with 4 keV Ar^+ ions incident at an angle of 70° with respect to the surface

[a]Author to whom correspondence should be addressed.

normal. Ti 2p, Ti 3s, Ti 3p, Al 2p, Al 2s, N 1s, and valence band spectra are presented.

The Ti 2p core-level spectra exhibit a satellite peak on the high binding energy (BE) side of the Ti $2p_{3/2}$ and Ti $2p_{1/2}$ peaks in agreement with earlier XPS analyses of TiN and TiAlN (Refs. 18–20). The origin of this feature is widely discussed in the literature and several interpretations have been proposed including intra-band transitions (shake-up events) (Refs. 19 and 21), a decrease in the screening of the core-hole due to photoionization (Refs. 18, 20, and 22), and structural effects (Ref. 23). Our data show that the relative intensity of the primary Ti 2p peaks with respect to that of the satellite features decreases with increasing AlN concentration and the satellite dominates the Ti 2p XPS spectra for samples with $x \geq 0.67$. At even higher AlN concentrations, $x \geq 0.96$, the primary Ti $2p_{3/2}$ and Ti $2p_{1/2}$ peaks are absent.

The above changes in the Ti 2p core level peaks are accompanied by a corresponding evolution of satellite features on the high-BE side of Ti 3s and Ti 3p peaks. $Ti_{1-x}Al_xN$ valence band spectra reveal that the density-of-states (DOS) at the Fermi level decrease with increasing x, indicating that the appearance of Ti satellite features is due to core-hole screening. The higher the density of occupied states at the Fermi level, the more effective the screening and hence, the higher the intensity of the primary core-level Ti peaks.

AlN concentrations obtained using XPS Ti 2p and Al 2p XPS sensitivity factors (Ref. 24) agree to within ±3%, with ToF-E ERDA results over the entire $Ti_{1-x}Al_xN$ alloy range $0 \leq x \leq 0.96$.

SPECIMEN DESCRIPTION (ACCESSION #01289, 1 OF 13) –

Host Material: TiN

Host Material Characteristics: homogeneous; solid; polycrystalline; conductor; inorganic compound; thin film

Chemical Name: titanium nitride

Source: Thin films are grown by reactive magnetron sputter deposition using a combination of high-power pulsed magnetron (HIPIMS) and DC magnetron sputtering (DCMS) from elemental Ti and Al targets.

Host Composition: titanium, nitrogen

Form: polycrystalline thin film

As Received Condition: as grown

Analyzed Region: not specified

***Ex Situ* Preparation/Mounting:** $Ti_{1-x}Al_xN$ ($0 \leq x \leq 0.96$) thin films are grown on Si(001) substrates at 500 °C by hybrid reactive Ti-HIPIMS/Al-DCMS co-sputtering from elemental Ti and Al targets (Refs. 14 and 15). Film growth is carried out in mixed Ar/N_2 atmospheres at a total pressure of 3 mTorr with a N_2/Ar flow ratio of 0.2. A bias of −60 V is applied to the substrate in synchronous with the HIPIMS pulses (Ref. 25). Except for $Ti_{1-x}Al_xN$ layers with AlN concentrations $x > 0.80$, film composition is controlled by varying the power P_{dc} to the dc magnetron from 0 kW (x = 0) to 3 kW (x = 0.80), while maintaining the average HIPIMS power P_{HIPIMS} constant at 5 kW (10 J/pulse, 500 Hz, 10% duty cycle). For growth of $Ti_{1-x}Al_xN$ layers with $x > 0.80$, P_{HIPIMS} is decreased to 2.5 kW (5 J/pulse, 500 Hz, 10% duty cycle) and P_{dc} is set at 2.5 (x = 0.92) and 3 kW (x = 0.96).

***In Situ* Preparation:** Prior to XPS analyses, TiAlN surfaces are sputter-cleaned with 4 keV Ar^+ ions incident at 70° with respect to the surface normal. The ion current density is 12.7 mA/cm^2 and the beam is rastered over a 2×2 mm^2 area for two min, corresponding to the removal of 32 nm from a polycrystalline Ta_2O_5 reference sample. XPS spectra are obtained from a 0.3×0.7 mm^2 area at the center of the sputter-cleaned region.

Pre-Analysis Beam Exposure: not applicable, sample insensitive to X-rays

Charge Control: No charge compensation was used during measurements. C 1s recorded prior to sputtering was only used to confirm calibration of the binding energy scale. Spectra included in this submission are after sputter-cleaning and are not shifted in any way from the original positions. This is because we find that the position of the Fermi Level cut-off coincides with "0" of the binding energy scale.

Temp. During Analysis: 300 K

Pressure During Analysis: $<1 \times 10^{-7}$ Pa

SPECIMEN DESCRIPTION (ACCESSION #01290, 2 OF 13) —

Host Material: $Ti_{0.84}Al_{0.16}N$

SPECIMEN DESCRIPTION (ACCESSION #01291, 3 OF 13) —

Host Material: $Ti_{0.74}Al_{0.26}N$

SPECIMEN DESCRIPTION (ACCESSION #01292, 4 OF 13) —

Host Material: $Ti_{0.65}Al_{0.35}N$

SPECIMEN DESCRIPTION (ACCESSION #01293, 5 OF 13) —

Host Material: $Ti_{0.59}Al_{0.41}N$

SPECIMEN DESCRIPTION (ACCESSION #01294, 6 OF 13) —

Host Material: $Ti_{0.46}Al_{0.54}N$

SPECIMEN DESCRIPTION (ACCESSION #01295, 7 OF 13) —

Host Material: $Ti_{0.41}Al_{0.59}N$

SPECIMEN DESCRIPTION (ACCESSION #01296, 8 OF 13) —

Host Material: $Ti_{0.33}Al_{0.67}N$

SPECIMEN DESCRIPTION (ACCESSION #01297, 9 OF 13) —

Host Material: $Ti_{0.27}Al_{0.73}N$

SPECIMEN DESCRIPTION (ACCESSION #01298, 10 OF 13) —

Host Material: $Ti_{0.24}Al_{0.76}N$

SPECIMEN DESCRIPTION (ACCESSION #01299, 11 OF 13) —

Host Material: $Ti_{0.20}Al_{0.80}N$

SPECIMEN DESCRIPTION (ACCESSION #01300, 12 OF 13) ——

Host Material: $Ti_{0.08}Al_{0.92}N$

SPECIMEN DESCRIPTION (ACCESSION #01301, 13 OF 13)

Host Material: $Ti_{0.04}Al_{0.96}N$

INSTRUMENT PARAMETERS COMMON TO ALL SPECTRA

■ Spectrometer

Analyzer Mode: constant pass energy

Throughput ($T=E^N$): N=0

Excitation Source Window: not specified

Excitation Source: Al K_α, monochromatic

Source Energy: 1486.6 eV

Source Strength: 225 W

Signal Mode: multichannel direct

■ Geometry

Incident Angle: 54°

Source to Analyzer Angle: 54°

Emission Angle: 0°

Specimen Azimuthal Angle: 90°

Acceptance Angle from Analyzer Axis: 0°

Analyzer Angular Acceptance Width: 30° × 30°

■ Ion Gun

Manufacturer and Model: Kratos Analytical MiniBeam IV

Energy: 4000 eV

Current: 12.7 mA/cm^2

Current Measurement Method: Faraday cup

Sputtering Species: Ar^+

Spot Size (unrastered): 200 μm

Raster Size: 2000 μm × 2000 μm

Incident Angle: 70°

Polar Angle: 70°

Azimuthal Angle: 180°

Comment: equivalent Ta_2O_5 sputter rate: 16 nm/min; sputtering performed with a differentially pumped ion gun

DATA ANALYSIS METHOD

Energy Scale Correction: No correction necessary. The position of the Fermi Level cut-off coincides with "0" of the binding energy scale.

Recommended Energy Scale Shift: none

Intensity Scale Correction: No correction necessary; all spectra were acquired under exactly the same conditions (during one day).

Peak Shape and Background Method: N/A

Quantitation Method: Quantification is performed with CasaXPS (version 2.3.16) software and is based on regions defined in narrow scans using Shirley background function.

Sensitivity factors are supplied by Kratos Analytical Ltd. (library file name: "casaXPS_KratosAxis-F1s.lib" - in this table the sensitivity factor for the F 1s peak is set to 1).

The Kratos sensitivity factors relate to both components of a spin-orbit split doublet. Following the nomenclature used by Kratos, sensitivity factor is only listed with the major component of the two peaks but this is the value used for BOTH components to get proper composition.

ACKNOWLEDGMENTS

Financial support from the European Research Council (ERC) through an Advanced Grant, the VINN Excellence Center Functional Nanoscale Materials (FunMat), the Knut and Alice Wallenberg Foundation, and the Strategic Faculty Grant In Materials Science (AFM) is gratefully acknowledged.

REFERENCES

1. O. Knotek, M. Böhmer, and T. Leyendecker, J. Vac. Sci. Technol., A **4**, 2695 (1986).
2. T. Leyendecker, O. Lemmer, S. Esser, and J. Ebberink, Surf. Coat. Technol. **48**, 175 (1991).
3. B. Subramanian, C. V. Muraleedharan, R. Ananthakumar, and M. Jayachandran, Surf. Coat. Technol. **205**, 5014 (2011).
4. F. Adibi, I. Petrov, L. Hultman, U. Wahlström, T. Shimizu, D. McIntyre, and J. E. Greene, J. Appl. Phys. **69**, 6437 (1991).
5. J. S. Schuster and J. Bauer, J. Solid State Chem. **53**, 260 (1984).
6. H. Holleck, Surf. Coat. Technol. **36**, 151 (1988).
7. B. Alling, A. V. Ruban, A. Karimi, O. E. Peil, S. I. Simak, L. Hultman, and I. A. Abrikosov, Phys. Rev. B **75**, 045123 (2007).
8. U. Wahlström, L. Hultman, J.-E. Sundgren, F. Adibi, I. Petrov, and J. E. Greene, Thin Solid Films **235**, 62 (1993).
9. F. Adibi, I. Petrov, J. E. Greene, U. Wahlstrom, and J.-E. Sundgren, J. Vac. Sci. Technol., A **11**, 136 (1993)
10. A. Hörling, L. Hultman, M. Odén, J. Sjölén, and L. Karlsson, J. Vac. Sci. Technol., A **20**, 1815 (2002).
11. T. Ikeda and H. Satoh, Thin Solid Films **195**, 99 (1991).
12. H. Oettel, R. Wiedemann, and S. Preisler, Surf. Coat. Technol. **74–75**, 273 (1995).
13. C. V. Falub, A. Karimi, M. Ante, and W. Kalss, Surf. Coat. Technol. **201**, 5891 (2007).
14. G. Greczynski, J. Lu, M. Johansson, J. Jensen, I. Petrov, J. E. Greene, and L. Hultman, Vacuum **86**, 1036 (2012).
15. G. Greczynski, J. Lu, M. Johansson, J. Jensen, I. Petrov, J. E. Greene, and L. Hultman, Surf. Coat. Technol. **206**, 4202 (2012).
16. G. Greczynski, J. Lu, J. Jensen, I. Petrov, J. E. Greene, S. Bolz, W. Kölker, Ch. Schiffers, O. Lemmer, and L. Hultman, Thin Solid Films **556**, 87 (2014).
17. J. Jensen, D. Martin, A. Surpi, and T. Kubart, Nucl. Instrum. Methods B **268**, 1893 (2010).
18. L. Porte, L. Roux, and J. Hanus, Phys. Rev. B **28**, 3214 (1983).
19. I. Strydom and S. Hofmann, J. Electron Spectrosc. Relat. Phenom. **56**, 85 (1991).
20. J. Patscheider, N. Hellgren, R. T. Haasch, I. Petrov, and J. E. Greene, Phys. Rev. B **83**, 125124 (2011).
21. D. Jaeger and J. Patscheider, J. Electron Spectrosc. Relat. Phenom. **185**, 523 (2012).
22. A. Arranz and C. Palacio, Surf. Sci. **600**, 2510 (2006).
23. P. Prieto and R. E. Kirby, J. Vac. Sci. Technol., A **13**, 2819 (1995).
24. Kratos Analytical, Ltd. Library filename: casaXPS_KratosAxis-F1s.lib.
25. G. Greczynski, J. Lu, J. Jensen, I. Petrov, J. E. Greene, S. Bolz, W. Kölker, Ch. Schiffers, O. Lemmer, and L. Hultman, J. Vac. Sci. Technol., A **30**, 061504 (2012).

SPECTRAL FEATURES TABLE

Spectrum ID #	Element/ Transition	Peak Energy (eV)	Peak Width FWHM (eV)	Peak Area (eV × cts/s)	Sensitivity Factor	Concentration (at. %)	Peak Assignment
Accession#-02[a]	Al 2p	74.2 to 74.3	1.3 to 1.4	0 to 18.6	0.193	0 to 50.24	Al in TiAlN
Accession#-03	Al 2s	119.1 to 119.3	1.7 to 1.8	0 to 19.6	···	···	Al in TiAlN
Accession#-04	N 1s	397.1 to 397.5	1.3 to 1.4	35 to 50	0.477	47.6 to 51.7	N in TiAlN
Accession#-05[b]	Ti $2p_{3/2}$	455.2	···	···	2.0	2.1 to 48.3	Ti in TiAlN
Accession#-05[c]	Ti $2p_{1/2}$	461.1	···	···	···	···	Ti in TiAlN
Accession#-05[d]	Ti $2p_{3/2}$	457.2 to 457.6	···	···	···	···	Ti in TiAlN
Accession#-05[e]	Ti $2p_{1/2}$	463.0 to 463.5	···	···	···	···	Ti in TiAlN
Accession#-06[f]	Ti 3p	34.6	···	···	···	···	Ti in TiAlN
Accession#-06[g]	Ti 3p	36.6	···	···	···	···	Ti in TiAlN
Accession#-07[h]	Ti 3s	59.8	···	···	···	···	Ti in TiAlN
Accession#-07[i]	Ti 3s	61.4	···	···	···	···	Ti in TiAlN

[a] quantification is based upon the area under the Al 2p peak envelope
[b] Ti $2p_{3/2}$ main line
[c] Ti $2p_{1/2}$ main line
[d] Ti $2p_{3/2}$ satellite feature
[e] Ti $2p_{1/2}$ satellite feature
[f] Ti 3p main line
[g] Ti 3p satellite feature
[h] Ti 3s main line
[i] Ti 3s satellite feature

This submission reports on 13 separate samples (Accession #s 1289 through 1301) of $Ti_{1-x}Al_xN$, with $0 \leq x \leq 0.96$. Table entries given as ranges, e.g. 119.1 to 119.3, reflect dependency on the value of x.

GUIDE TO FIGURES

Spectrum (Accession) #	Spectral Region	Voltage Shift*	Multiplier	Baseline	Comment #
1289-01	survey	0	1	0	1
1290-01	survey	0	1	−200	2
1291-01	survey	0	1	−400	3
1292-01	survey	0	1	−600	4
1293-01	survey	0	1	−800	5
1294-01	survey	0	1	−1000	6
1295-01	survey	0	1	−1200	7
1296-01	survey	0	1	−1400	8
1297-01	survey	0	1	−1600	9
1298-01	survey	0	1	−1800	10
1299-01	survey	0	1	−2000	11
1300-01	survey	0	1	−2200	12
1301-01	survey	0	1	−2400	13
1289-02	Al 2p	0	1	0	1
1290-02	Al 2p	0	1	0	2
1291-02	Al 2p	0	1	0	3
1292-02	Al 2p	0	1	0	4
1293-02	Al 2p	0	1	0	5
1294-02	Al 2p	0	1	0	6
1295-02	Al 2p	0	1	0	7
1296-02	Al 2p	0	1	0	8
1297-02	Al 2p	0	1	0	9
1298-02	Al 2p	0	1	0	10
1299-02	Al 2p	0	1	0	11
1300-02	Al 2p	0	1	0	12
1301-02	Al 2p	0	1	0	13
1289-03	Al 2s	0	1	0	1
1290-03	Al 2s	0	1	0	2
1291-03	Al 2s	0	1	0	3
1292-03	Al 2s	0	1	0	4
1293-03	Al 2s	0	1	0	5
1294-03	Al 2s	0	1	0	6
1295-03	Al 2s	0	1	0	7
1296-03	Al 2s	0	1	0	8
1297-03	Al 2s	0	1	0	9
1298-03	Al 2s	0	1	0	10
1299-03	Al 2s	0	1	0	11
1300-03	Al 2s	0	1	0	12
1301-03	Al 2s	0	1	0	13
1289-04	N 1s	0	1	0	1
1290-04	N 1s	0	1	0	2
1291-04	N 1s	0	1	0	3
1292-04	N 1s	0	1	0	4
1293-04	N 1s	0	1	0	5
1294-04	N 1s	0	1	0	6
1295-04	N 1s	0	1	0	7

SPECTRAL FEATURES TABLE (CONT.)

Spectrum (Accession) #	Spectral Region	Voltage Shift*	Multiplier	Baseline	Comment #
1296-04	N 1s	0	1	0	8
1297-04	N 1s	0	1	0	9
1298-04	N 1s	0	1	0	10
1299-04	N 1s	0	1	0	11
1300-04	N 1s	0	1	0	12
1301-04	N 1s	0	1	0	13
1289-05	Ti $2p_{1/2}$, Ti $2p_{3/2}$	0	1	0	1
1290-05	Ti $2p_{1/2}$, Ti $2p_{3/2}$	0	1	0	2
1291-05	Ti $2p_{1/2}$, Ti $2p_{3/2}$	0	1	0	3
1292-05	Ti $2p_{1/2}$, Ti $2p_{3/2}$	0	1	0	4
1293-05	Ti $2p_{1/2}$, Ti $2p_{3/2}$	0	1	0	5
1294-05	Ti $2p_{1/2}$, Ti $2p_{3/2}$	0	1	0	6
1295-05	Ti $2p_{1/2}$, Ti $2p_{3/2}$	0	1	0	7
1296-05	Ti $2p_{1/2}$, Ti $2p_{3/2}$	0	1	0	8
1297-05	Ti $2p_{1/2}$, Ti $2p_{3/2}$	0	1	0	9
1298-05	Ti $2p_{1/2}$, Ti $2p_{3/2}$	0	1	0	10
1299-05	Ti $2p_{1/2}$, Ti $2p_{3/2}$	0	1	0	11
1300-05	Ti $2p_{1/2}$, Ti $2p_{3/2}$	0	1	0	12
1301-05	Ti $2p_{1/2}$, Ti $2p_{3/2}$	0	1	0	13
1289-06	Ti 3p	0	1	0	1
1290-06	Ti 3p	0	1	0	2
1291-06	Ti 3p	0	1	0	3
1292-06	Ti 3p	0	1	0	4
1293-06	Ti 3p	0	1	0	5
1294-06	Ti 3p	0	1	0	6
1295-06	Ti 3p	0	1	0	7
1296-06	Ti 3p	0	1	0	8
1297-06	Ti 3p	0	1	0	9
1298-06	Ti 3p	0	1	0	10
1299-06	Ti 3p	0	1	0	11
1300-06	Ti 3p	0	1	0	12
1301-06	Ti 3p	0	1	0	13
1289-07	Ti 3s	0	1	0	1
1290-07	Ti 3s	0	1	0	2
1291-07	Ti 3s	0	1	0	3
1292-07	Ti 3s	0	1	0	4
1293-07	Ti 3s	0	1	0	5
1294-07	Ti 3s	0	1	0	6
1295-07	Ti 3s	0	1	0	7
1296-07	Ti 3s	0	1	0	8
1297-07	Ti 3s	0	1	0	9
1298-07	Ti 3s	0	1	0	10
1299-07	Ti 3s	0	1	0	11
1300-07	Ti 3s	0	1	0	12
1301-07	Ti 3s	0	1	0	13
1289-08	valence band	0	1	0	1

SPECTRAL FEATURES TABLE (CONT.)

Spectrum (Accession) #	Spectral Region	Voltage Shift*	Multiplier	Baseline	Comment #
1290-08	valence band	0	1	0	2
1291-08	valence band	0	1	0	3
1292-08	valence band	0	1	0	4
1293-08	valence band	0	1	0	5
1294-08	valence band	0	1	0	6
1295-08	valence band	0	1	0	7
1296-08	valence band	0	1	0	8
1297-08	valence band	0	1	0	9
1298-08	valence band	0	1	0	10
1299-08	valence band	0	1	0	11
1300-08	valence band	0	1	0	12
1301-08	valence band	0	1	0	13

* Voltage shift of the archived (as-measured) spectrum relative to the printed figure. The figure reflects the recommended energy scale correction due to a calibration correction, sample charging, flood gun, or other phenomenon.

1. TiN
2. $Ti_{0.84}Al_{0.16}N$
3. $Ti_{0.74}Al_{0.26}N$
4. $Ti_{0.65}Al_{0.35}N$
5. $Ti_{0.59}Al_{0.41}N$
6. $Ti_{0.46}Al_{0.54}N$
7. $Ti_{0.41}Al_{0.59}N$
8. $Ti_{0.33}Al_{0.67}N$
9. $Ti_{0.27}Al_{0.73}N$
10. $Ti_{0.24}Al_{0.76}N$
11. $Ti_{0.20}Al_{0.80}N$
12. $Ti_{0.08}Al_{0.92}N$
13. $Ti_{0.04}Al_{0.96}N$

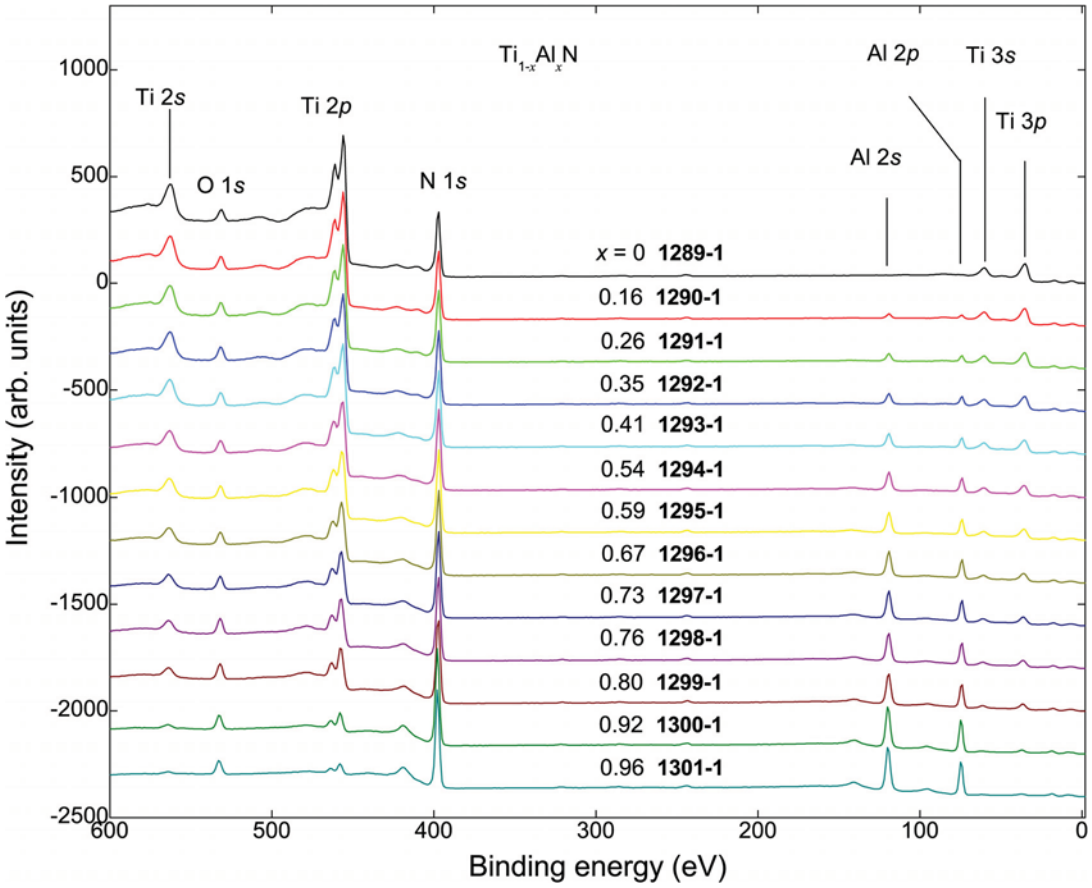

Accession #	**01289–01**, **01290–01**, **01291–01**, **01292–01**, **01293–01**, **01294–01**, **01295–01**, **01296–01**, **01297–01**, **01298–01**, **01299–01**, **01300–01**, **01301–01**
Host Material	#01289-01: TiN; #01290-01: $Ti_{0.84}Al_{0.16}N$; #01291-01: $Ti_{0.74}Al_{0.26}N$; #01292-01: $Ti_{0.65}Al_{0.35}N$; #01293-01: $Ti_{0.59}Al_{0.41}N$; #01294-01: $Ti_{0.46}Al_{0.54}N$; #01295-01: $Ti_{0.41}Al_{0.59}N$; #01296-01: $Ti_{0.33}Al_{0.67}N$; #01297-01: $Ti_{0.27}Al_{0.73}N$; #01298-01: $Ti_{0.24}Al_{0.76}N$; #01299-01: $Ti_{0.20}Al_{0.80}N$; #01300-01: $Ti_{0.08}Al_{0.92}N$; #01301-01: $Ti_{0.04}Al_{0.96}N$
Technique	XPS
Spectral Region	survey
Instrument	Kratos Analytical Axis Ultra DLD
Excitation Source	Al K_α monochromatic
Source Energy	1486.6 eV
Source Strength	225 W
Source Size	2 mm × 2 mm
Analyzer Type	hemispherical analyzer, mean radius: 165 mm
Incident Angle	54°
Emission Angle	0°
Analyzer Pass Energy:	160 eV
Analyzer Resolution	1.6 eV
Total Signal Accumulation Time	302 s
Total Elapsed Time	not specified
Number of Scans	1
Effective Detector Width	16 eV

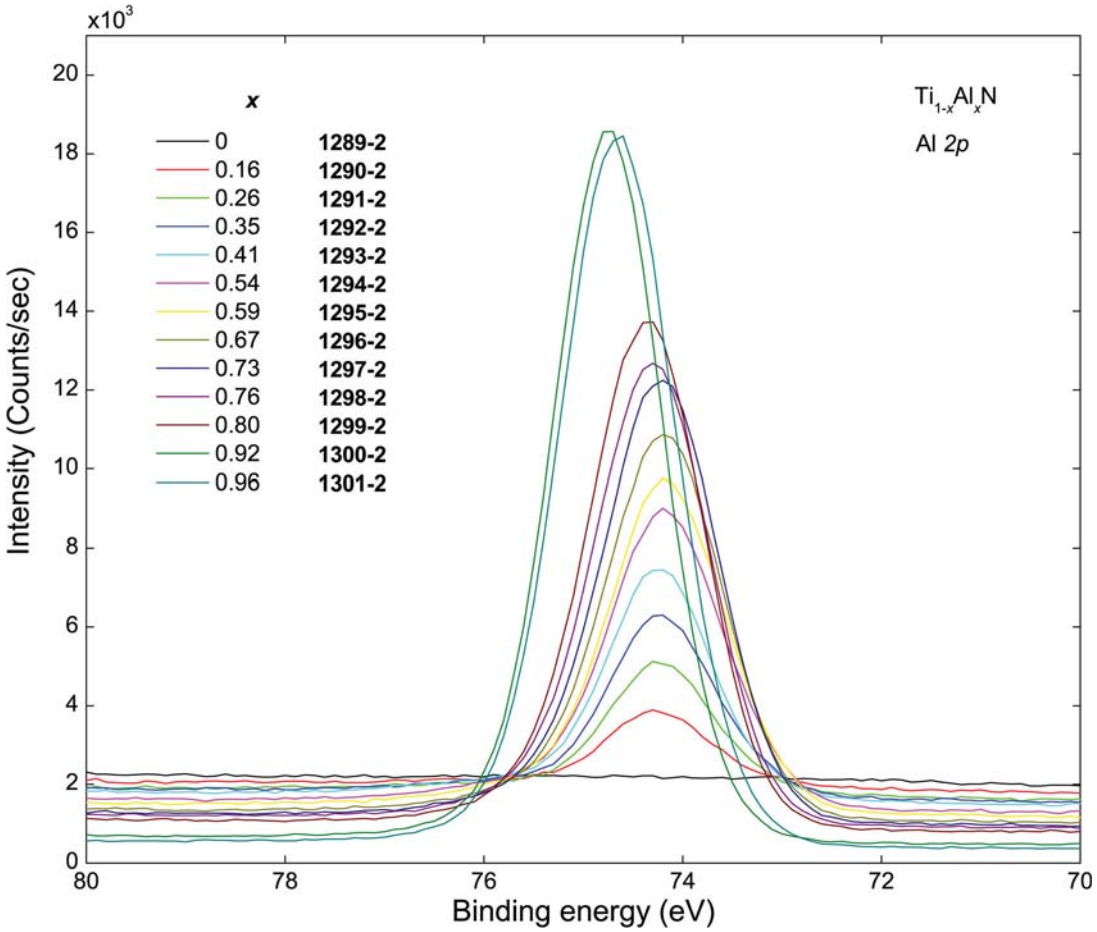

Accession #	**01289–02, 01290–02, 01291–02, 01292–02, 01293–02, 01294–02, 01295–02, 01296–02, 01297–02, 01298–02, 01299–02, 01300–02, 01301–02**
Host Material	#01289-02: TiN; #01290-02: $Ti_{0.84}Al_{0.16}N$; #01291-02: $Ti_{0.74}Al_{0.26}N$; #01292-02: $Ti_{0.65}Al_{0.35}N$; #01293-02: $Ti_{0.59}Al_{0.41}N$; #01294-02: $Ti_{0.46}Al_{0.54}N$; #01295-02: $Ti_{0.41}Al_{0.59}N$; #01296-02: $Ti_{0.33}Al_{0.67}N$; #01297-02: $Ti_{0.27}Al_{0.73}N$; #01298-02: $Ti_{0.24}Al_{0.76}N$; #01299-02: $Ti_{0.20}Al_{0.80}N$; #01300-02: $Ti_{0.08}Al_{0.92}N$; #01301-02: $Ti_{0.04}Al_{0.96}N$
Technique	XPS
Spectral Region	Al 2*p*
Instrument	Kratos Analytical Axis Ultra DLD
Excitation Source	Al K_α monochromatic
Source Energy	1486.6 eV
Source Strength	225 W
Source Size	2 mm × 2 mm
Analyzer Type	hemispherical analyzer, mean radius: 165 mm
Incident Angle	54°
Emission Angle	0°
Analyzer Pass Energy:	20 eV
Analyzer Resolution	0.20 eV
Total Signal Accumulation Time	303 s
Total Elapsed Time	not specified
Number of Scans	10
Effective Detector Width	2 eV

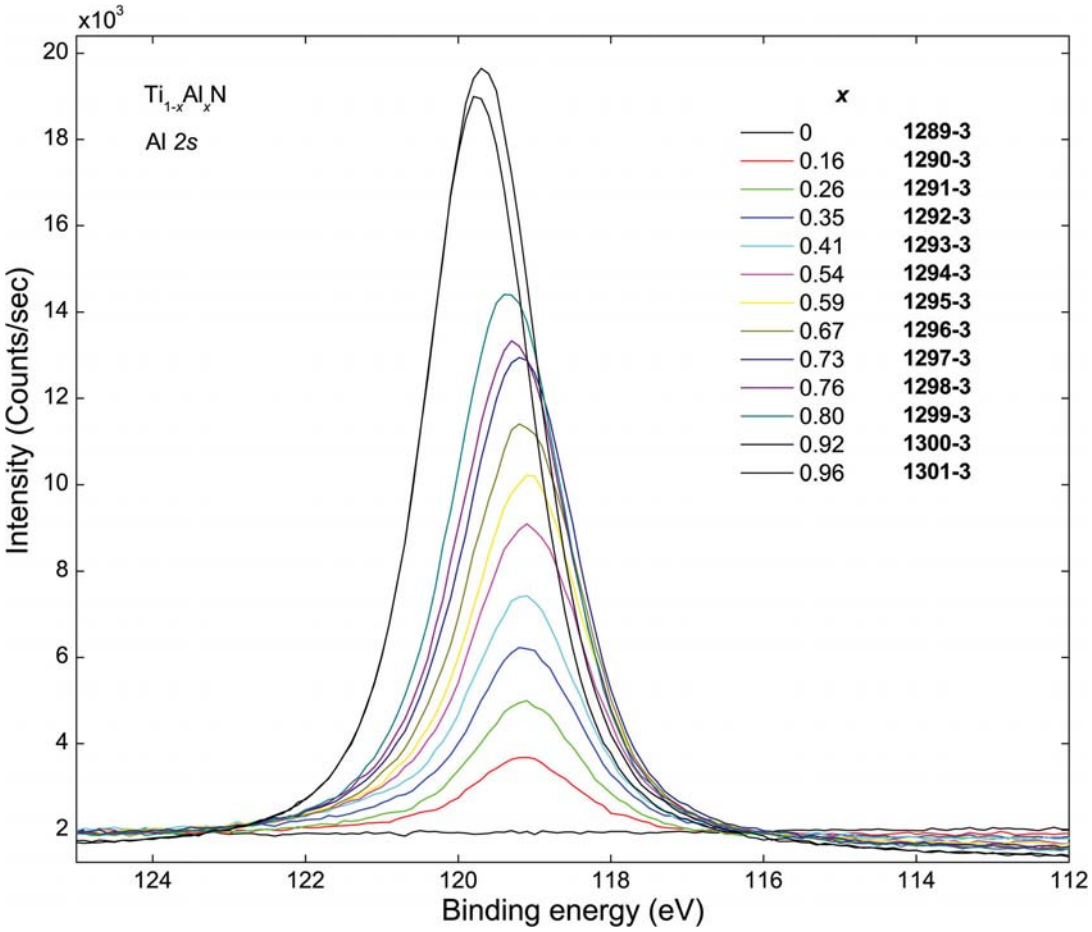

Accession #	**01289–03, 01290–03, 01291–03, 01292–03, 01293–03, 01294–03, 01295–03, 01296–03, 01297–03, 01298–03, 01299–03, 01300–03, 01301–03**
Host Material	#01289-03: TiN; #01290-03: $Ti_{0.84}Al_{0.16}N$; #01291-03: $Ti_{0.74}Al_{0.26}N$; #01292-03: $Ti_{0.65}Al_{0.35}N$; #01293-03: $Ti_{0.59}Al_{0.41}N$; #01294-03: $Ti_{0.46}Al_{0.54}N$; #01295-03: $Ti_{0.41}Al_{0.59}N$; #01296-03: $Ti_{0.33}Al_{0.67}N$; #01297-03: $Ti_{0.27}Al_{0.73}N$; #01298-03: $Ti_{0.24}Al_{0.76}N$; #01299-03: $Ti_{0.20}Al_{0.80}N$; #01300-03: $Ti_{0.08}Al_{0.92}N$; #01301-03: $Ti_{0.04}Al_{0.96}N$
Technique	XPS
Spectral Region	Al 2*s*
Instrument	Kratos Analytical Axis Ultra DLD
Excitation Source	Al K_α monochromatic
Source Energy	1486.6 eV
Source Strength	225 W
Source Size	2 mm × 2 mm
Analyzer Type	hemispherical analyzer, mean radius: 165 mm
Incident Angle	54°
Emission Angle	0°
Analyzer Pass Energy:	20 eV
Analyzer Resolution	0.20 eV
Total Signal Accumulation Time	423 s
Total Elapsed Time	not specified
Number of Scans	10
Effective Detector Width	2 eV

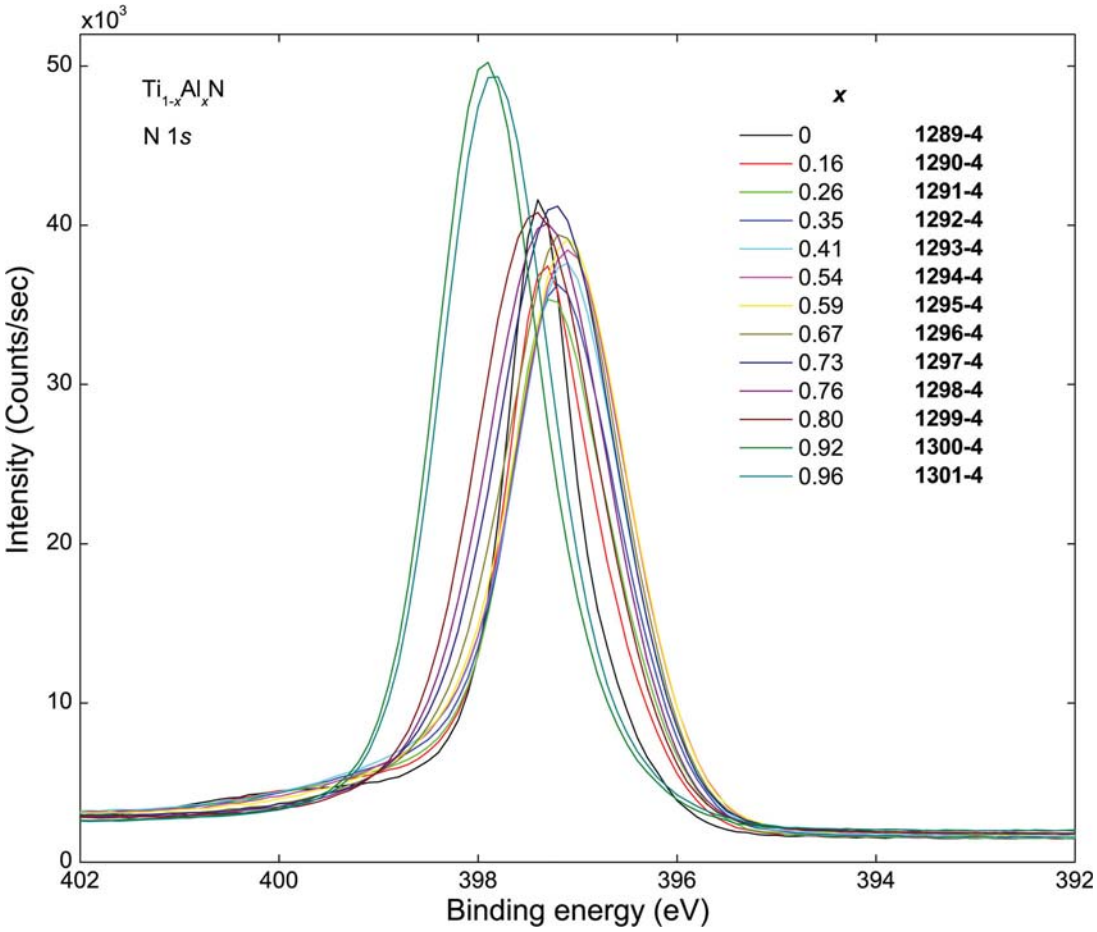

Accession #	**01289–04**, **01290–04**, **01291–04**, **01292–04**, **01293–04**, **01294–04**, **01295–04**, **01296–04**, **01297–04**, **01298–04**, **01299–04**, **01300–04**, **01301–04**
Host Material	#01289-04: TiN; #01290-04: $Ti_{0.84}Al_{0.16}N$; #01291-04: $Ti_{0.74}Al_{0.26}N$; #01292-04: $Ti_{0.65}Al_{0.35}N$; #01293-04: $Ti_{0.59}Al_{0.41}N$; #01294-04: $Ti_{0.46}Al_{0.54}N$; #01295-04: $Ti_{0.41}Al_{0.59}N$; #01296-04: $Ti_{0.33}Al_{0.67}N$; #01297-04: $Ti_{0.27}Al_{0.73}N$; #01298-04: $Ti_{0.24}Al_{0.76}N$; #01299-04: $Ti_{0.20}Al_{0.80}N$; #01300-04: $Ti_{0.08}Al_{0.92}N$; #01301-04: $Ti_{0.04}Al_{0.96}N$
Technique	XPS
Spectral Region	N 1*s*
Instrument	Kratos Analytical Axis Ultra DLD
Excitation Source	Al K_α monochromatic
Source Energy	1486.6 eV
Source Strength	225 W
Source Size	2 mm × 2 mm
Analyzer Type	hemispherical analyzer, mean radius: 165 mm
Incident Angle	54°
Emission Angle	0°
Analyzer Pass Energy:	20 eV
Analyzer Resolution	0.20 eV
Total Signal Accumulation Time	361 s
Total Elapsed Time	not specified
Number of Scans	10
Effective Detector Width	2 eV

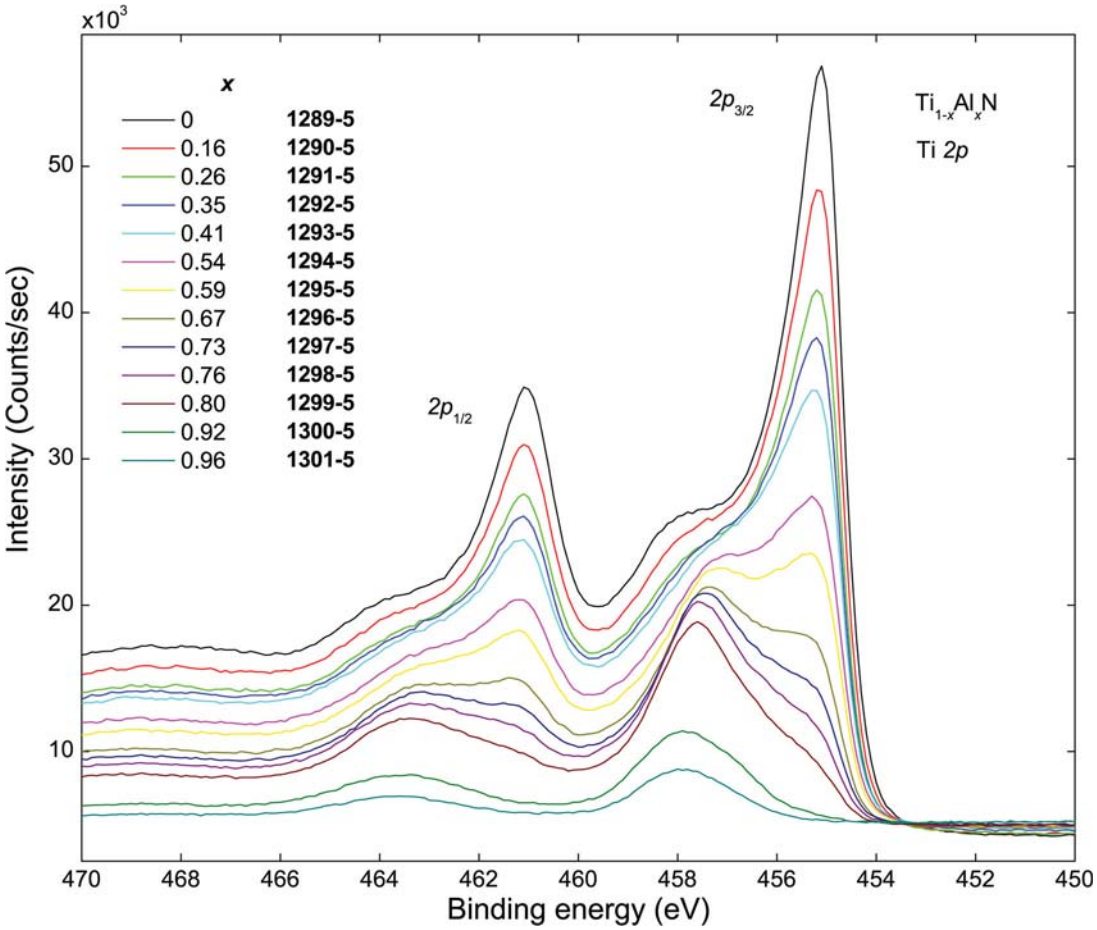

Accession #	**01289–05**, **01290–05**, **01291–05**, **01292–05**, **01293–05**, **01294–05**, **01295–05**, **01296–05**, **01297–05**, **01298–05**, **01299–05**, **01300–05**, **01301–05**
Host Material	#01289-05: TiN; #01290-05: $Ti_{0.84}Al_{0.16}N$; #01291-05: $Ti_{0.74}Al_{0.26}N$; #01292-05: $Ti_{0.65}Al_{0.35}N$; #01293-05: $Ti_{0.59}Al_{0.41}N$; #01294-05: $Ti_{0.46}Al_{0.54}N$; #01295-05: $Ti_{0.41}Al_{0.59}N$; #01296-05: $Ti_{0.33}Al_{0.67}N$; #01297-05: $Ti_{0.27}Al_{0.73}N$; #01298-05: $Ti_{0.24}Al_{0.76}N$; #01299-05: $Ti_{0.20}Al_{0.80}N$; #01300-05: $Ti_{0.08}Al_{0.92}N$; #01301-05: $Ti_{0.04}Al_{0.96}N$
Technique	XPS
Spectral Region	Ti $2p_{1/2}$; Ti $2p_{3/2}$
Instrument	Kratos Analytical Axis Ultra DLD
Excitation Source	Al K_α monochromatic
Source Energy	1486.6 eV
Source Strength	225 W
Source Size	2 mm × 2 mm
Analyzer Type	hemispherical analyzer, mean radius: 165 mm
Incident Angle	54°
Emission Angle	0°
Analyzer Pass Energy:	20 eV
Analyzer Resolution	0.20 eV
Total Signal Accumulation Time	606 s
Total Elapsed Time	not specified
Number of Scans	10
Effective Detector Width	2 eV

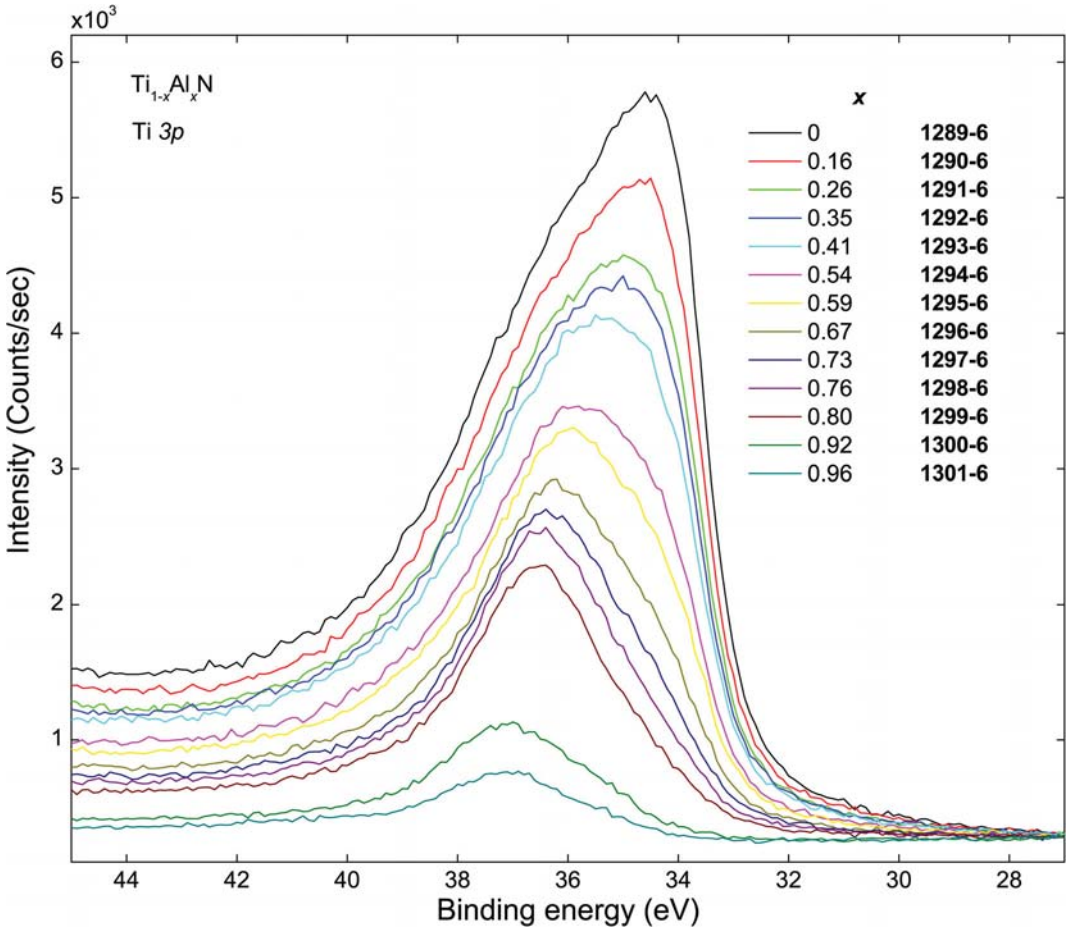

Accession #	**01289–06**, **01290–06**, **01291–06**, **01292–06**, **01293–06**, **01294–06**, **01295–06**, **01296–06**, **01297–06**, **01298–06**, **01299–06**, **01300–06**, **01301–06**
Host Material	#01289-06: TiN; #01290-06: $Ti_{0.84}Al_{0.16}N$; #01291-06: $Ti_{0.74}Al_{0.26}N$; #01292-06: $Ti_{0.65}Al_{0.35}N$; #01293-06: $Ti_{0.59}Al_{0.41}N$; #01294-06: $Ti_{0.46}Al_{0.54}N$; #01295-06: $Ti_{0.41}Al_{0.59}N$; #01296-06: $Ti_{0.33}Al_{0.67}N$; #01297-06: $Ti_{0.27}Al_{0.73}N$; #01298-06: $Ti_{0.24}Al_{0.76}N$; #01299-06: $Ti_{0.20}Al_{0.80}N$; #01300-06: $Ti_{0.08}Al_{0.92}N$; #01301-06: $Ti_{0.04}Al_{0.96}N$
Technique	XPS
Spectral Region	Ti 3*p*
Instrument	Kratos Analytical Axis Ultra DLD
Excitation Source	Al K_α monochromatic
Source Energy	1486.6 eV
Source Strength	225 W
Source Size	2 mm × 2 mm
Analyzer Type	hemispherical analyzer, mean radius: 165 mm
Incident Angle	54°
Emission Angle	0°
Analyzer Pass Energy:	20 eV
Analyzer Resolution	0.20 eV
Total Signal Accumulation Time	573 s
Total Elapsed Time	not specified
Number of Scans	10
Effective Detector Width	2 eV

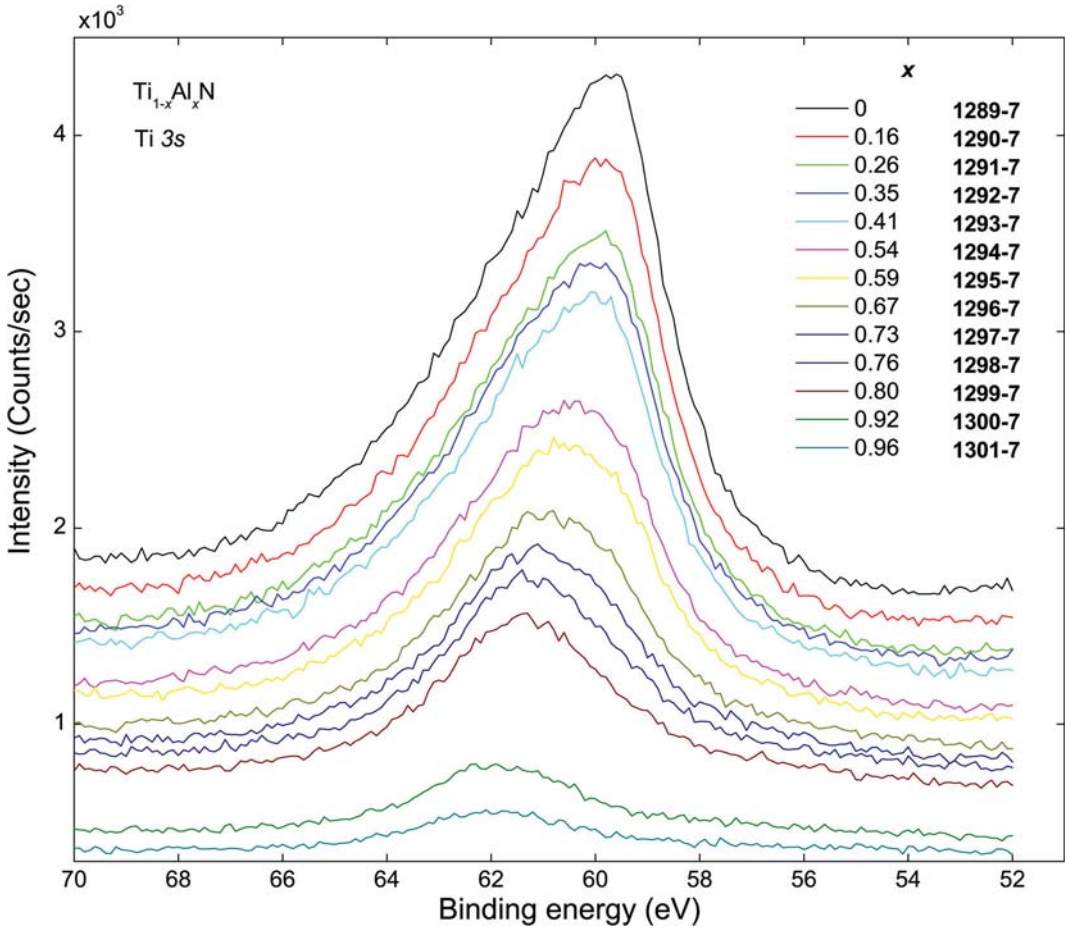

Accession #	**01289–07, 01290–07, 01291–07, 01292–07, 01293–07, 01294–07, 01295–07, 01296–07, 01297–07, 01298–07, 01299–07, 01300–07, 01301–07**
Host Material	#01289-07: TiN; #01290-07: $Ti_{0.84}Al_{0.16}N$; #01291-07: $Ti_{0.74}Al_{0.26}N$; #01292-07: $Ti_{0.65}Al_{0.35}N$; #01293-07: $Ti_{0.59}Al_{0.41}N$; #01294-07: $Ti_{0.46}Al_{0.54}N$; #01295-07: $Ti_{0.41}Al_{0.59}N$; #01296-07: $Ti_{0.33}Al_{0.67}N$; #01297-07: $Ti_{0.27}Al_{0.73}N$; #01298-07: $Ti_{0.24}Al_{0.76}N$; #01299-07: $Ti_{0.20}Al_{0.80}N$; #01300-07: $Ti_{0.08}Al_{0.92}N$; #01301-07: $Ti_{0.04}Al_{0.96}N$
Technique	XPS
Spectral Region	Ti 3*s*
Instrument	Kratos Analytical Axis Ultra DLD
Excitation Source	Al K_α monochromatic
Source Energy	1486.6 eV
Source Strength	225 W
Source Size	2 mm × 2 mm
Analyzer Type	hemispherical analyzer, mean radius: 165 mm
Incident Angle	54°
Emission Angle	0°
Analyzer Pass Energy:	20 eV
Analyzer Resolution	0.20 eV
Total Signal Accumulation Time	543 s
Total Elapsed Time	not specified
Number of Scans	10
Effective Detector Width	2 eV

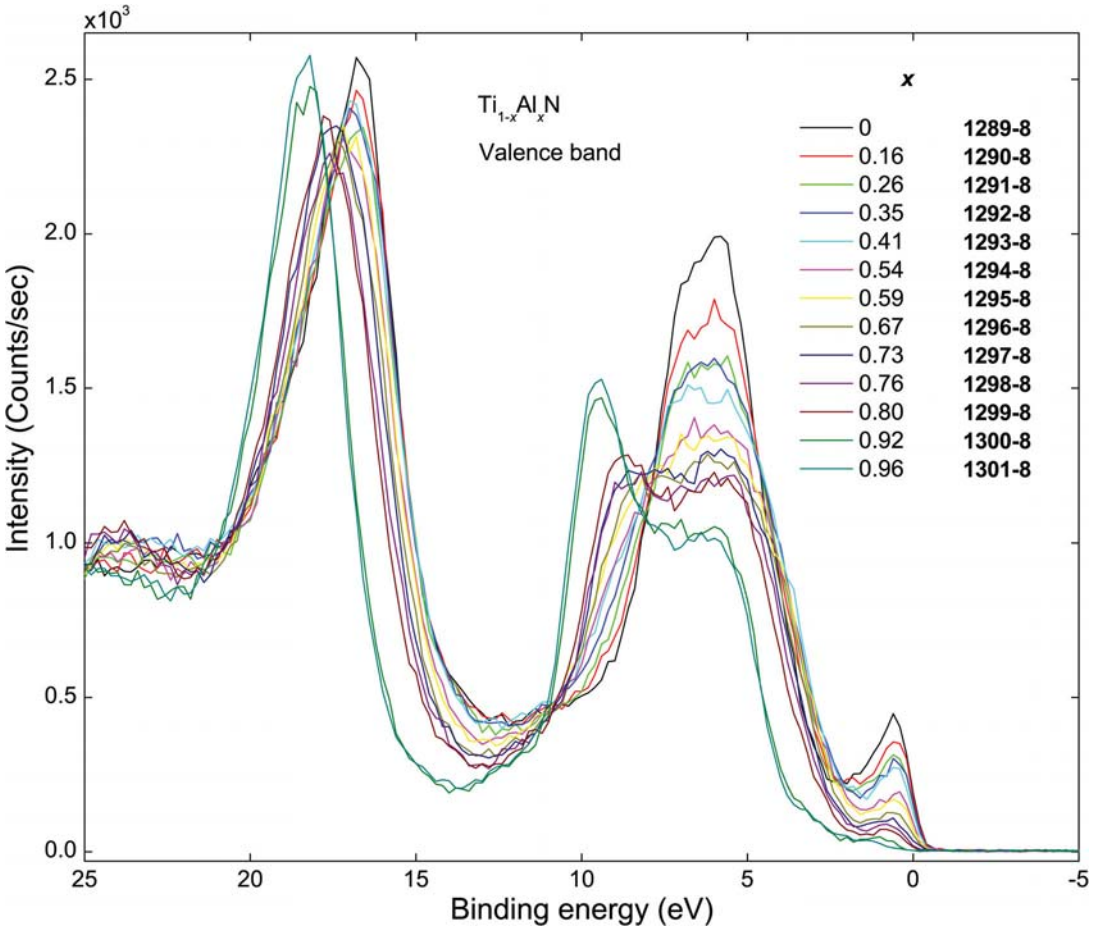

Accession #	**01289–08**, **01290–08**, **01291–08**, **01292–08**, **01293–08**, **01294–08**, **01295–08**, **01296–08**, **01297–08**, **01298–08**, **01299–08**, **01300–08**, **01301–08**
Host Material	#01289-08: TiN; #01290-08: $Ti_{0.84}Al_{0.16}N$; #01291-08: $Ti_{0.74}Al_{0.26}N$; #01292-08: $Ti_{0.65}Al_{0.35}N$; #01293-08: $Ti_{0.59}Al_{0.41}N$; #01294-08: $Ti_{0.46}Al_{0.54}N$; #01295-08: $Ti_{0.41}Al_{0.59}N$; #01296-08: $Ti_{0.33}Al_{0.67}N$; #01297-08: $Ti_{0.27}Al_{0.73}N$; #01298-08: $Ti_{0.24}Al_{0.76}N$; #01299-08: $Ti_{0.20}Al_{0.80}N$; #01300-08: $Ti_{0.08}Al_{0.92}N$; #01301-08: $Ti_{0.04}Al_{0.96}N$
Technique	XPS
Spectral Region	valence band
Instrument	Kratos Analytical Axis Ultra DLD
Excitation Source	Al K_α monochromatic
Source Energy	1486.6 eV
Source Strength	225 W
Source Size	not specified
Analyzer Type	hemispherical analyzer, mean radius: 165 mm
Incident Angle	54°
Emission Angle	0°
Analyzer Pass Energy:	40 eV
Analyzer Resolution	0.40 eV
Total Signal Accumulation Time	302 s
Total Elapsed Time	not specified
Number of Scans	10
Effective Detector Width	4 eV